Manipulation of cellulose nanocrystal surface sulfate groups towards biomimetic nanostructures in aqueous media

Justin O. Zoppe,[‡,]* Leena-Sisko Johansson,[±] and Jukka Seppälä[†]

[‡]Institut des Matériaux and Institut des Sciences et Ingénierie Chimiques, Laboratoire des Polymères, École Polytechnique Fédérale de Lausanne (EPFL), Bâtiment MXD, Station 12, CH-1015 Lausanne, Switzerland

[†]Polymer Technology, Department of Biotechnology & Chemical Technology, Aalto University School of Chemical Technology, P.O. Box 16100, 00076 Aalto, Finland

[±]Department of Forest Products Technology, Aalto University School of Chemical Technology, P.O. Box 16300, 00076 Aalto, Finland

*Corresponding author E-mail: justin.zoppe@epfl.ch, Phone: +41 21 693 4872, Fax: + 41 21 693 5650

KEYWORDS. Cellulose nanocrystals, whiskers, desulfation, tyrosine sulfate mimetics, multivalent nanoparticles, sulfonated ligands, polyanionic inhibitors.

ABSTRACT

We report a facile aqueous procedure to create multivalent displays of sulfonated ligands on CNCs for future applications as viral inhibitors. CNCs were decorated with model compounds containing sulfonate groups via reactions of epoxides and isothiocyanates with amines under alkaline conditions. At first, surface sulfate groups of CNCs were hydrolytically cleaved by alkaline hydrolysis to increase the number of available surface hydroxyls. Success of desulfation was confirmed via dynamic light scattering (DLS), zeta potential measurements and thermogravimetric analysis (TGA). CNC surface hydroxyl groups were then activated with epichlorohydrin before subsequent reactions. As proof of concept towards aqueous pathways for functionalizing nanoparticles with sulfonated ligands, 3-chloro-2-hydroxy-1-propanesulfonic acid sodium salt hydrate (CPSA) and 4-sulfophenyl isothiocyanate sodium salt monohydrate (4-SPITC) were chosen as model compounds to react with homobifunctional 2,2'-(ethylenedioxy)bis(ethylamine) (EBEA) molecular spacer. The approaches presented are not only applicable to polysaccharide nanocrystals, but also other classes of polymeric and inorganic substrates presenting surface hydroxyl groups, as in the case of poly(2-hydroxyethyl methacrylate) (PHEMA), silica or glass. CNCs carrying sulfonated ligands were characterized by ATR-FTIR and UV-Vis spectroscopy. Surface chemical compositions of desired elements were determined via X-ray Photoelectron Spectroscopy (XPS). We anticipate that with these facile aqueous procedures as the proof of concept, a diverse library of target-specific functionalities can be conjugated to CNCs for applications in nanomedicine, especially related to viral inhibition.

1. Introduction

Sulfation of biomolecules plays central roles in biological processes such as the regulation of receptor-ligand binding, cell signaling and adhesion, the solubilization of xenobiotics, and regulation of cancer cells (Grunwell & Bertozzi, 2002). Sulfation is regulated by sulfotransferase enzymes, which transfer a sulfonate group to an alcohol or amino functionality present in carbohydrates, proteins, or other small molecules. More specifically, sulfation of tyrosine residues is an essential post-translational modification linked to high affinity electrostatic binding events (Stone, Chuang, Hou, Shoham & Zhu, 2009). For example, P-selectin glycoprotein ligand-1 (PSGL-1) binding with P-selectin for cell adhesion processes requires sulfated tyrosine residues. Furthermore, sulfated tyrosines at the N-terminus of C-C chemokine receptor type 5 (CCR5) promote human immunodeficiency virus-1 (HIV-1) entry into host cells (Farzan et al., 1999). Cell surface heparan sulfate (HS) presents multiple sulfate groups involved in cell signal transduction, receptor-mediated endocytosis and membrane fusion of viruses (Bernfield et al., 1999). Although sulfate and sulfonate functional groups have slightly different polarities and acid-base chemistry, they are, nevertheless, structurally similar, such that sulfonate groups can be used to effectively mimic the sulfate groups present in various biomolecules. As a result, novel nanotechnologies have been applied to combat various types of viral infections in the laboratory setting, such as tyrosine sulfate mimicking small molecules (Acharya et al., 2011) and multivalent nanoparticles carrying sulfate (Di Gianvincenzo, Marradi, Martinez-Avila, Bedoya, Alcami & Penades, 2010), sulfonate (Baram-Pinto, Shukla, Gedanken & Sarid, 2010; Baram-Pinto, Shukla, Perkas, Gedanken & Sarid, 2009) and phenyl sulfonate groups (Zoppe et al., 2014).

Anionic polysaccharide derivatives have a long history of antiviral activity, especially sulfated polysaccharides such as carregeenan and cellulose sulfate (Pirrone, Wigdahl & Krebs, 2011; Yamamoto et al., 1991). In the case of cellulose sulfate, derivatization of hydroxyl groups has

typically been carried out by chlorosulfonic acid treatment, sulfuric acid and isopropyl alcohol mixtures, or sulfur trioxide complexes (Gericke, Liebert & Heinze, 2009). On the other hand, polysaccharides can be derivatized under milder conditions by the use of epoxides or isothiocyanates (Hermanson, 2008). Cellulose nanocrystals (CNCs), also produced from sulfuric acid hydrolysis, form highly stable aqueous dispersions, as a result of electrostatic stabilization imparted by surface sulfate groups (Habibi, Lucia & Rojas, 2010; Moon, Martini, Nairn, Simonsen & Youngblood, 2011). The biocompatibility of CNCs has been demonstrated against multiple cell lines (Dong, Hirani, Colacino, Lee & Roman, 2012; Jackson, Letchford, Wasserman, Ye, Hamad & Burt, 2011; Lam, Male, Chong, Leung & Luong, 2012; Male, Leung, Montes, Kamen & Luong, 2012; Ni et al., 2012; Zoppe et al., 2014), thus represent an attractive candidate as a carrier of biomimetic functional groups for applications in nanomedicine. Numerous hydroxyl functionalities offer the base for further conjugation of target-specific molecules. Dong et al. (Dong & Roman, 2007) introduced fluorescent labels onto CNCs via hydroxyl group activation with epichlorohydrin, followed by amination and subsequent conjugation with fluorescein-5'-isothiocyanate (FITC). Later, Nielsen et al. (Nielsen, Eyley, Thielemans & Aylott, 2010) demonstrated that isothiocyanates can be reacted directly with CNC surface hydroxyl groups under similar conditions to create ratiometric pH sensing systems.

Recently, our group demonstrated that CNCs functionalized with multivalent displays of sulfate or phenyl sulfonate moieties inhibit Semliki Forest Virus (SFV) infection and do not induce significant cytotoxicity, in agreement with previous studies (Dong, Hirani, Colacino, Lee & Roman, 2012; Zoppe et al., 2014). However, the creation of CNCs carrying phenyl sulfonate ligands involved laborious solvent exchange steps and multi-step synthesis in organic media, which may hinder the sustainability and scalability of the process. In this report, we propose a simplified aqueous procedure to create multivalent displays of sulfonated ligands on CNCs targeted for

antiviral applications. The approaches presented are not only applicable to polysaccharide nanocrystals, but also other classes of polymeric and inorganic substrates presenting surface hydroxyl groups, as in the case of poly(2-hydroxyethyl methacrylate) (PHEMA), silica or glass (Haensch, Hoeppener & Schubert, 2010; Hermanson, 2008). Herein, CNCs were decorated with model compounds containing sulfonate groups via reactions of epoxides and isothiocyanates with a homobifunctional amine molecular spacer under alkaline conditions. Surface sulfate groups of CNCs were hydrolytically cleaved by alkaline hydrolysis in order to increase the number of available surface hydroxyl groups. Success of the desulfation reaction was confirmed via dynamic light scattering (DLS), zeta potential measurements and thermogravimetric analysis (TGA). CNC surface hydroxyl groups were first activated with epichlorohydrin before subsequent reactions. Surface chemical compositions of sulfur and nitrogen were determined via X-ray Photoelectron Spectroscopy (XPS). CNCs carrying sulfonated ligands were also characterized by ATR-FTIR and UV-Vis spectroscopy. We hope that with simple aqueous procedures as a proof of concept, a diverse library of biomimetic functionalities can be conjugated to CNCs for potential applications in nanomedicine.

2. Materials & Methods

2.1. Materials. Sulfuric acid (95%) and acetone (99%) were purchased from VWR Scientific. Cotton fibers were purchased from a local grocery store (Espoo, Finland). Dialysis tubing cellulose membrane (MWCO 12,400), epichlorohydrin, 3-chloro-2-hydroxy-1-propanesulfonic acid sodium salt hydrate (CPSA), 4-sulfophenyl isothiocyanate sodium salt monohydrate (4-SPITC), and 2,2'-(ethylenedioxy)bis(ethylamine) (EBEA) were all purchased from Sigma-Aldrich.

2.2. Production of cellulose nanocrystals (CNCs). CNCs were extracted from cotton fibers by acid hydrolysis via 65 wt% aqueous sulfuric acid solution at 45 °C for 45 minutes. The resulting dispersion of CNCs was diluted with distilled water and filtered into ~200 g ice cubes to quench the

hydrolysis reaction. CNCs were washed with distilled water by successive centrifugations at 12,000 rpm at 4 °C for 20 minutes each. Subsequently, dialysis was carried out for one week against distilled water with a 12,400 MWCO dialysis membrane to remove residual sulfuric acid and by products. The concentration of the resulting CNCs dispersions were calculated gravimetrically.

2.3. Removal of cellulose nanocrystal sulfate groups. Sulfate groups were hydrolytically cleaved from CNCs following established procedures (Jiang, Esker & Roman, 2010; Kloser & Gray, 2010). 1 % wt. dispersions of CNCs were treated with 1 M NaOH at 60 °C for 5 hours. Then, the reaction was quenched by a 10-fold dilution with distilled water and centrifuged at 12,000 rpm at 4 °C for 20 minutes. Consequently, desulfated CNCs were re-dispersed and dialyzed against distilled water for one week to remove traces of NaOH. In the case of later epoxide functionalizations (section 2.4), the subsequent reaction was carried out immediately after desulfation in a one pot procedure.

2.4. Synthesis of sulfonated and phenyl sulfonated cellulose nanocrystals containing 2,2'-(ethylenedioxy)bis(ethylamine) (EBEA) molecular spacers in aqueous media. After the desulfation reaction, 2.0 molar equiv. of epichlorohydrin to anhydroglucose unit (AGU) were added in the same reaction vessel and stirred at 40 °C for 20 hours. Then, the reaction was diluted, centrifuged and re-dispersed, then brought to pH = 11 with a few drops of 1 M NaOH (referred to as compound **1**). Subsequently, 2.0 molar equiv. of EBEA was added and reacted at 40 °C for 20 hours. The reaction was then dialyzed for 24 hours to remove unreacted EBEA from solution and brought to pH = 11 (referred to as compound **2**). Then, 2.0 molar equiv. of either CPSA or 4-SPITC to AGU was added and reacted at 40 °C for another 20 hours. The products were then collected by centrifugation, re-dispersed and dialyzed for one week. These samples are referred to as compound **3** and **4**, respectively.

2.5. Dynamic light scattering (DLS) and Zeta potential measurements. Aqueous dispersions of unmodified CNCs and desulfated CNCs (0.1 % wt.) were analyzed in a Malvern Zetasizer Nano ZS at pH 7.1 and 0.01 M NaCl. All measurements were performed using a refractive index of 1.470 for

cellulose. CNCs dispersions were sonicated for 20 minutes immediately before DLS measurements in disposable cuvettes with a detection angle of 173° at room temperature. Z-average particle diameter values reported represent the diameter of equivalent spherical particles with the same translational diffusion coefficient. ζ-potential measurements were carried out in disposable folded capillary cells and electrophoretic mobilities were converted to ζ-potential using the Smoluchowski model with a Henry's function value of 1.50 (Hunter, 1981). All values reported are the average of three measurements.

2.6. Thermogravimetric analysis (TGA). Lyophilized samples of unmodified CNCs and desulfated CNCs were subjected to TGA analysis in a PerkinElmer TGA 4000. 2-5 mg of samples were placed in ceramic pans and weight loss was monitored from 30 to 600 °C at a rate of 10 °C/min under a nitrogen flow rate of 20 mL/min.

2.7. UV-Visible spectroscopy. Ultraviolet-visible spectroscopy was conducted on a UNICAM HELIOS β UV/Vis spectrophotometer. Transmission spectra of the samples in the wavelength range of 190 nm to 400 nm were collected with disposable polystyrene cuvettes containing aqueous dispersions of unmodified or modified CNCs at 0.1 % wt.

2.8. Attenuated Total Reflectance-Fourier Transform Infrared Spectroscopy (ATR-FTIR). Infrared spectra were obtained from freeze-dried samples were placed directly in a Mattson 3000 FTIR spectrometer equipped with a Pike Technologies GladiATR accessory. All spectra were collected with a 2 cm^{-1} resolution after 32 continuous scans.

2.9. X-Ray Photoelectron Spectroscopy. XPS measurements were performed on lyophilized samples of CNCs with an AXIS 165 electron spectrometer and monochromatic Al irradiation. Samples were evacuated overnight in order to stabilize vacuum conditions in the spectrometer. Samples were measured at three locations on the surface (analysis area of *ca.* 1 mm^2) and the

161 average values were recorded. Elemental surface compositions were determined from low-
162 resolution scans recorded with an 80 eV analyzer pass energy and a 1 eV step. Carbon high-
163 resolution spectra were recorded at binding energies in the C 1s region using 20 eV analyzer pass
164 energy and 0.1 eV step. Symmetric Gaussian components with Shirley background were used in the
165 curve fitting procedure for C 1s (Johansson & Campbell, 2004; Johansson, Campbell, Koljonen &
166 Stenius, 1999). The binding energy axis was shifted assuming the C-C binding energy at 285.0 eV
167 (Beamson & Briggs, 1992). Whatman filter paper reference standard was utilized as 100 %
168 cellulose.
169
170 3. **Results & Discussion**
171 ***3.1. Pathways to manipulate CNC sulfate groups.*** Polyanionic compounds and multivalent
172 nanoparticles carrying sulfate or phenyl sulfonate groups are highly effective viral inhibitors
173 (Baram-Pinto, Shukla, Gedanken & Sarid, 2010; Baram-Pinto, Shukla, Perkas, Gedanken & Sarid,
174 2009; Di Gianvincenzo, Marradi, Martinez-Avila, Bedoya, Alcami & Penades, 2010; Pirrone,
175 Wigdahl & Krebs, 2011; Yamamoto et al., 1991). In previous work, we have shown that CNCs
176 carrying multivalent displays of sulfate or phenyl sulfonate groups inhibited alphavirus infections
177 (Zoppe et al., 2014). The synthesis of CNCs carrying phenyl sulfonate ligands involved laborious
178 solvent exchange steps and multi-step synthesis in organic media, therefore we were motivated to
179 find simplified aqueous procedures to functionalize CNCs with multivalent displays. Accordingly,
180 CNCs were produced from cotton fiber by sulfuric acid hydrolysis with standard procedures. CNCs
181 produced from cotton generally have dimensions of ~4-7 nm in width and ~100-200 nm in length
182 (Habibi, Lucia & Rojas, 2010; Moon, Martini, Nairn, Simonsen & Youngblood, 2011). Additional
183 physical characterization of the resultant CNCs can be found in our previous work (Zoppe, Grosset
184 & Seppälä, 2013; Zoppe et al., 2014). Although CNCs already contain multivalent displays of
185 sulfate groups on their surfaces by the nature of sulfuric acid hydrolysis, previous studies have

shown a pronounced impact of molecular spacer length on binding affinities of biomolecules (Wang, Ramstrom & Yan, 2010). This could be due to a number of factors including, but not limited to ligand density and increased translational freedom associated with molecular spacer flexibility. Thus, including molecular spacers between CNC surfaces and anionic functional groups under aqueous conditions was a desirable approach. To increase the number of available surface hydroxyl groups on CNC surfaces for further functionalization, sulfate groups were hydrolytically cleaved before later reactions (Jiang, Esker & Roman, 2010; Kloser & Gray, 2010). The desulfation conditions used have been previously optimized to maximize the yield of desulfated CNCs without Mercerization, that is, doing little damage to their crystal structure as indicated by X-ray diffraction analysis (Lin & Dufresne, 2014). The success of desulfation was previously determined by conductometric titration, yielding 0.22 mequiv/g and 0.04 mequiv/g, unmodified CNCs and desulfated CNCs, respectively (Zoppe et al., 2014). In order to functionalize CNCs with EBEA molecular spacers in aqueous media, cotton CNC surfaces were first activated with epichlorohydrin to introduce epoxide groups following Dong *et al*. (Dong & Roman, 2007) with slight modifications (compound **1**). Epoxide-activated CNCs were then reacted with EBEA (compound **2**), followed by derivatization with CPSA or 4-SPITC, to yield compound **3** and **4**, respectively (shown in Scheme 1). CPSA has also been utilized to modify polyvinyl chloride sheets to facilitate surface-initiated atom transfer radical polymerization (SI-ATRP) in aqueous media (Zou, Kizhakkedathu & Brooks, 2009). Additionally, the proposed reaction scheme may potentially be carried out in a one pot procedure if compounds **2**, **3** and **4** are synthesized at 1 M NaOH, as in the case of compound **1**. However, for this proof of concept, the concentration was decreased to 1 mM NaOH by centrifugation and dilution steps to avoid undesired reactant consumption in solution following established bioconjugation protocols (Hermanson, 2008).

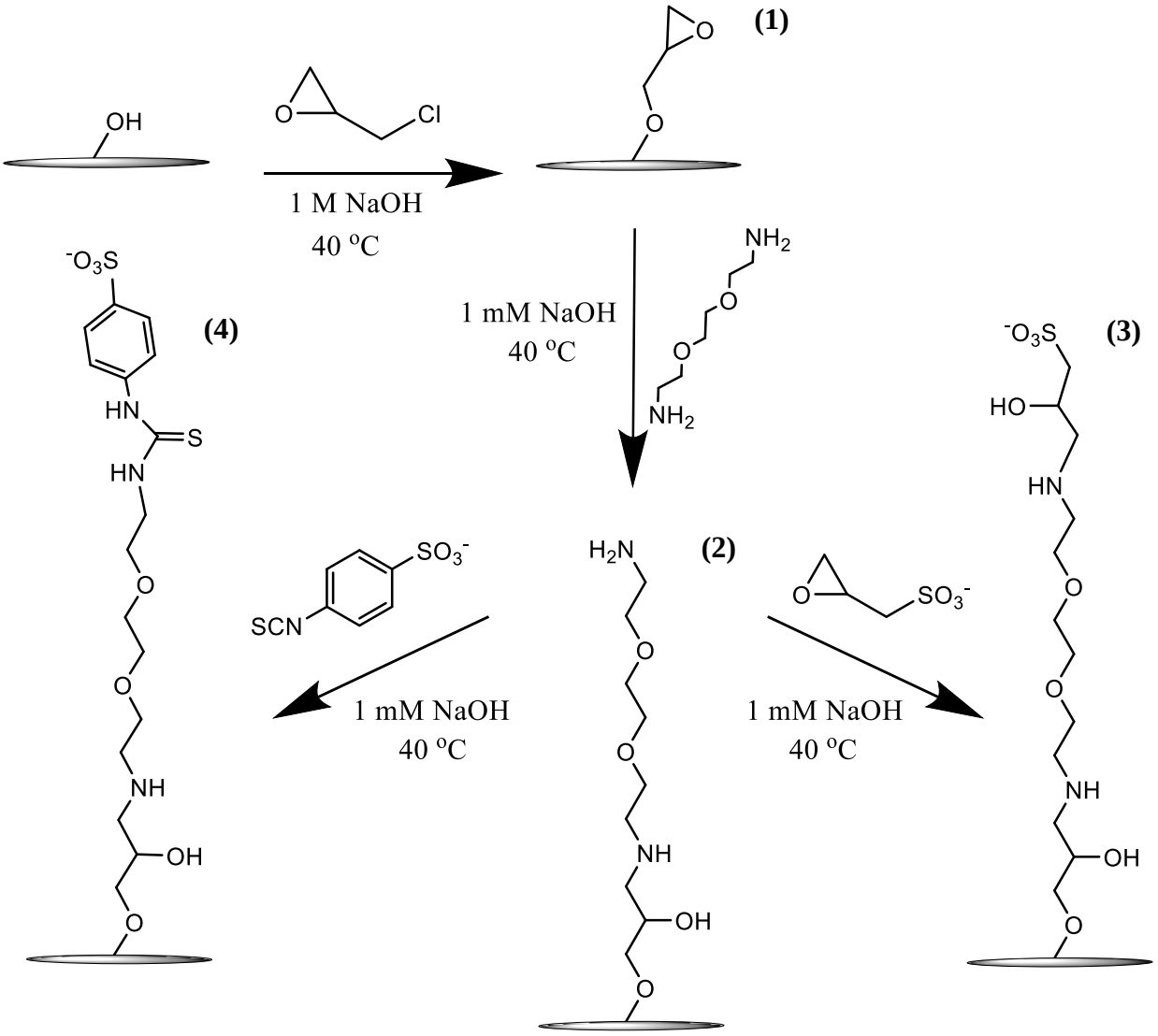

Scheme 1. Synthesis of cellulose nanocrystals carrying sulfonated ligands in aqueous media. (**1**) Surface hydroxyl groups activated with epichlorohydrin, (**2**) epoxide ring opening with 2,2'-(ethylenedioxy)bis(ethylamine) (EBEA), (**3**) amine addition reaction with 3-chloro-2-hydroxy-1-propanesulfonic acid sodium salt hydrate (CPSA), and (**4**) thiourea formation with 4-sulfophenyl isothiocyanate sodium salt monohydrate (4-SPITC).

3.2. ATR-FTIR spectroscopy characterization of CNCs carrying biomimetic sulfonate moieties. The reaction between epichlorohydrin and CNCs hydroxyl groups after desulfation was initially confirmed by ATR-FTIR spectroscopy (Figure 1). The spectrum of CNCs conjugated with epichlorohydrin (compound **1**) displayed notable changes in peak intensities within the range of 1500-1300 cm^{-1} when compared to unmodified CNCs. Increased peak intensities were observed at

1428 cm^{-1} and 1370 cm^{-1} corresponding to the epoxide group, in agreement with Müller *et al.* (Mueller et al., 2013) The peak at *ca.* 1650 cm^{-1} observed in the spectrum of compound 1 was assigned to -OH bending of residual water. Following the epoxide ring opening with EBEA (compound **2**), peaks within this range were reduced to intensities similar to that of unmodified CNCs. Given the presence of hydroxyl groups and glycosidic bonds throughout the cellulose chains within CNCs, it was difficult to resolve differences in FTIR spectra due to reaction with EBEA. However, the reduction in epoxide group peak intensity at 1428 cm^{-1} indicated that reaction with EBEA had occurred, due to the highly nucleophilic character of primary amines. In addition, thorough dialysis against distilled water was expected to sufficiently remove unreacted material following each reaction step for FTIR analysis, therefore the overall reduction in peak intensities within the range of 1500-1300 cm^{-1} qualitatively indicated the success of reactions. This was later confirmed by XPS (sections 3.3 and 3.5) after subsequent reactions with epoxides and isothiocyanates of CPSA and 4-SPITC, respectively.

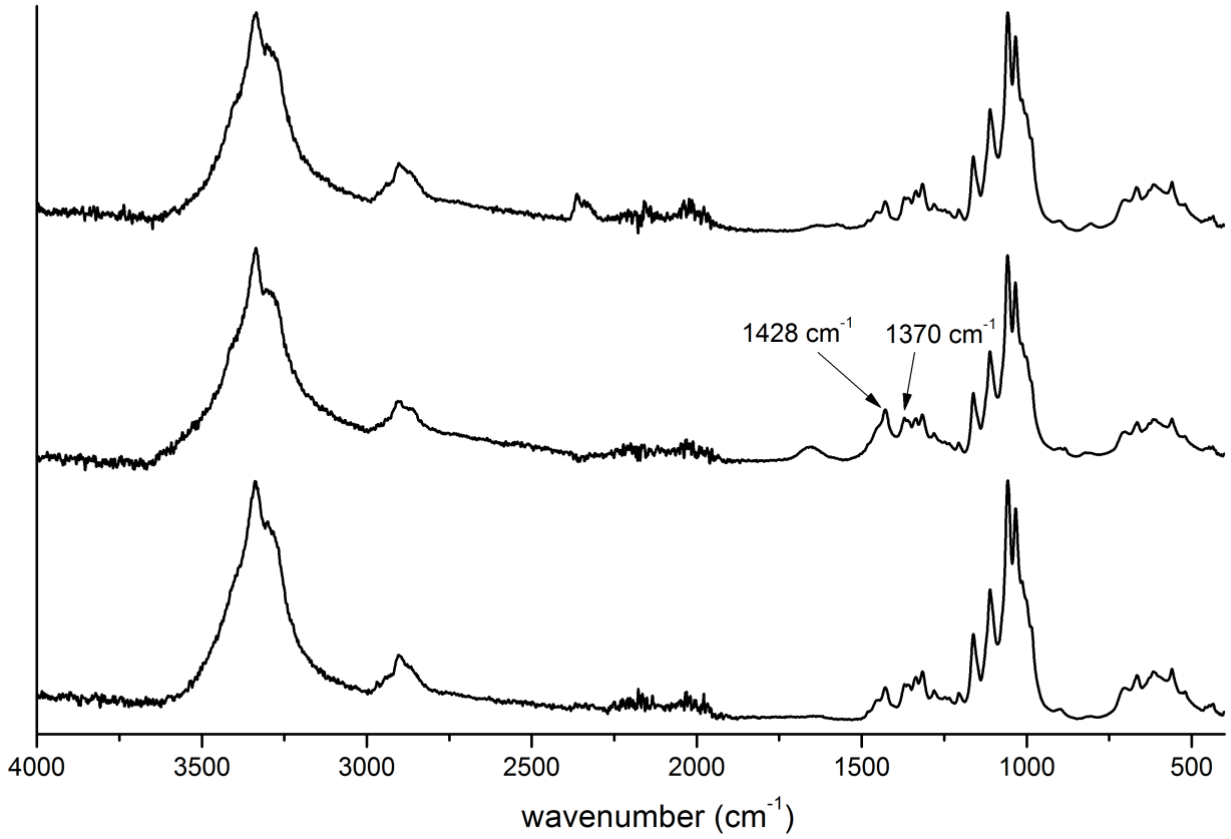

Figure 1. ATR-FTIR spectra of unmodified CNCs (bottom), compound **1** (middle) and compound **2** (top).

The exposed amine nucleophile of CNCs modified with EBEA (compound **2**) could be further reacted either with epoxides or isothiocyanates under alkali conditions (Hermanson, 2008). As proof of concept towards aqueous pathways for functionalizing nanoparticles with sulfonated ligands, CPSA was chosen as a model compound to react with exposed amines on CNC surfaces (compound **3**). The reaction between CPSA and the amine was initially confirmed by a C-N stretch at 1261 cm^{-1} (shown in Figure 2), which was also observed in our previous work (Zoppe et al., 2014). In addition, a strong peak at 801 cm^{-1} appeared and was assigned to the S-O stretch of sulfonate groups. This S-O stretch was also present at very low intensity in unmodified CNCs, seen at the bottom of Figure 2, due to surface sulfate groups from sulfuric acid hydrolysis. As previously discussed, modified CNC samples were thoroughly dialyzed against distilled water, therefore it was

considered unlikely that any adsorbed reactants would hinder our analysis since electrostatic repulsion would exist between negatively charged ligands and partially anionic CNC surfaces.

In addition to reactions with epoxides, surface amine groups of compound **2** were also reacted with 4-SPITC which resulted in a small, but measureable peak at 804 cm^{-1} assigned to C-H bending of aromatic rings in compound **4** (see Figure 2). The peak at 2380-2290 cm^{-1} observed in the spectrum of compound **4** was assigned to background carbon dioxide. In our previous work, reactions were carried out in DMSO via activation of CNC hydroxyl groups with 1,1'-carbonyldiimidazole (Zoppe et al., 2014). In that case, each reaction step could be easily resolved with FTIR due to shifts in carbonyl peaks and the appearance of an amine bend. On the contrary, here activation with epichlorohydrin and subsequent reaction steps could only be followed by changes in peak intensities in the 1500-1300 cm^{-1} region and by the appearance of aromatic C-H bends at 804 cm^{-1}. The same peak was also identified in our previous work when 4-SPITC was conjugated directly to CNC hydroxyl groups, although in the present case, we would argue that isothiocyanates preferentially reacted with primary amines rather than hydroxyl groups under these mildly basic conditions due to their stronger nucleophilic character. As mentioned before, unreacted chemicals were most likely removed by thorough dialysis of the modified CNC samples against distilled water; therefore it is expected that FTIR gave qualitative evidence for the presence of phenyl sulfonate groups, which was later confirmed by UV-Vis spectroscopy. All the aforementioned samples were subjected to conductometric titration in order to quantify the number of acidic groups, but they could not be detected. As was the case of prior reactions carried out in DMSO, likely only a limited degree of surface substitution was obtained and was therefore below the detection limit of our conductometric titration experiments. Nevertheless, even with low degrees of surface substitution, such biomimetic nanostructures can act as highly effective viral inhibitors (Zoppe et al., 2014).

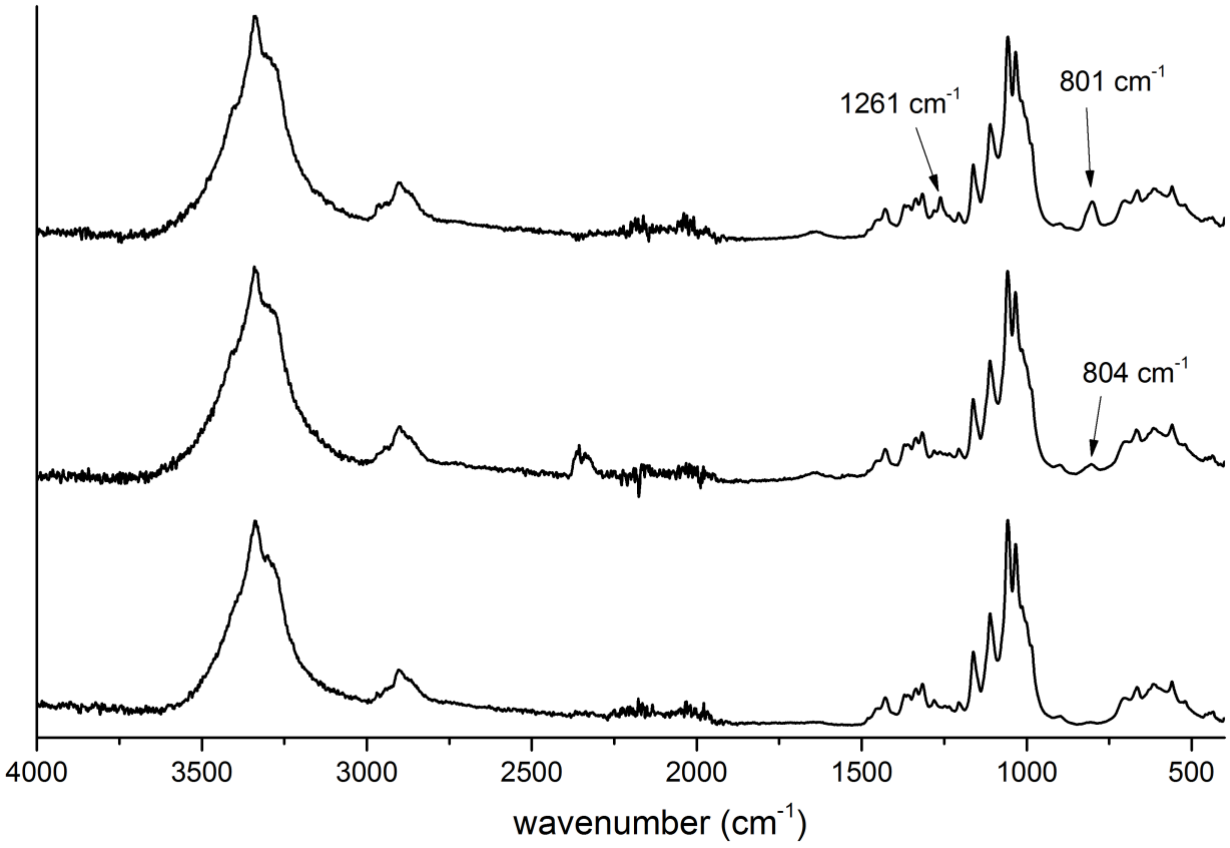

Figure 2. ATR-FTIR spectra of unmodified CNCs (bottom), compound **4** (middle) and compound **3** (top).

3.3. XPS characterization of S 2p. XPS experiments were also conducted in attempts to better quantify sulfonated ligands attached to CNCs. Wide scan XPS spectra and surface chemical compositions including oxygen, carbon, nitrogen and sulfur can be found in supporting information (Figure S1 and Table 1). Whatman filter paper was also analyzed as a reference standard (Johansson & Campbell, 2004). A detailed discussion of XPS results of unmodified and desulfated CNCs in comparison to the Whatman filter paper reference standard can be found in our previous work (Zoppe et al., 2014). Here, we focused on the N 1s and S 2p region of compounds **3** and **4** in comparison to desulfated CNCs. In addition, since the elemental quantities determined from the wide scan XPS spectra are strongly affected by impurities and since the C 1s signal is typically the most prone to contamination, we examined the ratios % S/O and % N/O to (shown in Table 1).

Initially, we expected to detect a significantly lower S 2p peak intensity for desulfated CNCs, shown in Figure 3, since our previous conductometric titrations determined only 0.04 mequiv/g of acidic groups (Zoppe et al., 2014). At first, the explanation for this discrepancy between conductometric titration and XPS eluded us and is discussed a greater detail in section 3.4. The subsequent XPS analysis of compounds **3** and **4** gave more conclusive results. Compound **3** showed an increase in sulfur peak intensity compared to desulfated CNCs. This increase in peak intensity was an indication of sulfonate groups after the reaction of CPSA with aminated CNCs, which was previously confirmed by FTIR (Figure 2). Compound **3** also displayed a % S/O ratio of 0.95, in comparison to 0.69 for desulfated CNCs, even though EBEA also partially contributed to the O 1s signal. The % N/O ratio also increased from 0.23 to 0.71, which suggested successful attachment of both EBEA, followed by CPSA, which is discussed in more detail in section 3.5. Interestingly, compound **4** presented two separate peaks within the S 2p region, attributed to two distinct sulfur species in the sample (bottom of Figure 3). The higher binding energy (~169 eV) corresponded to phenyl sulfonate groups, while the lower binding energy (~164 eV) corresponded to thiourea groups, which suggested the proposed structure of compound **4** in Scheme 1. On the other hand, the % S/O ratio of compound **4** was 0.47, which indicated an even lower sulfur content than desulfated CNCs, shown in Table 1. Yet, we observed a drastic increase in % N/O ratio, from 0.23 to 1.2, that also suggested the proposed structure of compound **4**. Clearly, there were inconsistencies between the expected and determined % sulfur in the samples, therefore we were driven to further investigate the efficiency of the desulfation reaction.

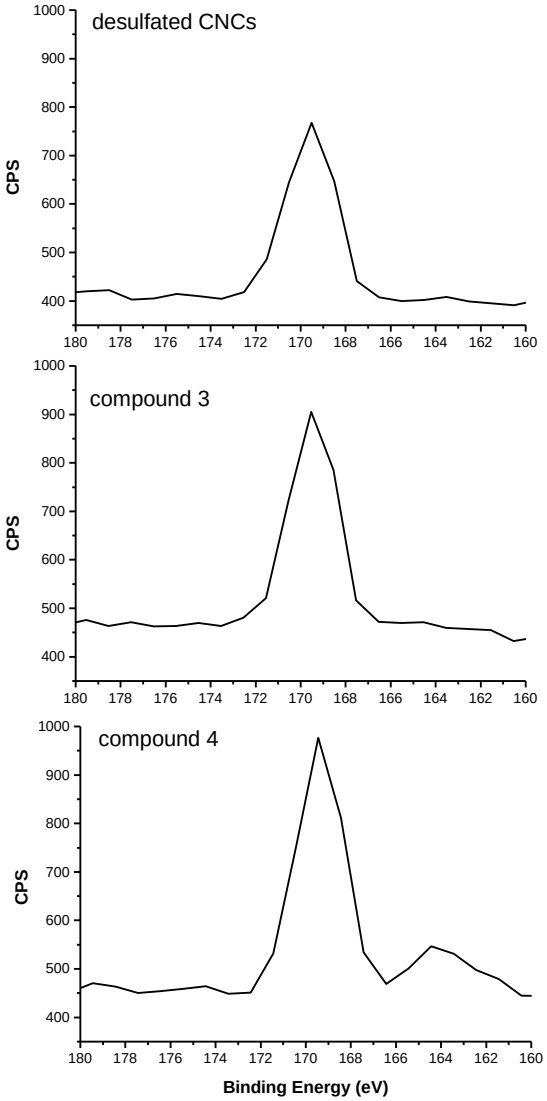

Figure 3. S 2p region of wide scan XPS spectra of desulfated CNCs (top), compound 3 (middle) and compound 4 (bottom).

Table 1. Summary of surface chemical composition of cotton CNCs before and after modifications determined from wide scan XPS spectra. S/O and N/O ratios are expressed as a percentage (*e.g.* (S 2p)/(O 1s) x 100).

Sample	O 1s (%)	C 1s (%)	Si 2p (%)	N 1s (%)	S 2p (%)	Na 1s (%)	O/C	S/O (%)	N/O (%)
Sulfated CNCs	42.4	56.8	0.8	-	0.3	-	0.75	0.71	-
Desulfated CNCs	43.5	55.7	0.1	0.1	0.3	0.3	0.78	0.69	0.23
3	42.3	56.5	0.6	0.3	0.4	-	0.75	0.95	0.71
4	42.9	56.0	0.2	0.5	0.2	0.3	0.77	0.47	1.2
Whatman reference	43.4	56.6	-	-	-	-	0.77	-	-

3.4. Chemical state of sulfur in CNCs after hydrolytic desulfation. As mentioned in the previous section, the relatively high intensity of the S 2p peak for desulfated CNCs was unexpected, based on the results of conductometric titrations (Zoppe et al., 2014). This anomaly posed the question: What is the chemical nature of the observed sulfur in "desulfated" CNCs? Previous work has shown the effectiveness of base-catalyzed hydrolytic desulfation to remove anionic sulfate groups (Kloser & Gray, 2010), although elemental analysis and XPS studies suggest a significant amount of sulfur is still present in "desulfated" CNCs (Jiang, Esker & Roman, 2010; Lin & Dufresne, 2014). In order to confirm previous observations, we conducted ζ-potential and dynamic light scattering (DLS) experiments to determine the electric potential at the slipping plane of the electrical double layer (EDL) at CNC surfaces and their colloidal aggregation behavior, respectively. Dispersions of unmodified CNCs and desulfated CNCs at pH 7.1 and 0.01 M NaCl displayed distinct results in both cases, as shown in Table 2. Unmodified CNCs gave a ζ-potential value of -36 mV, as a result of anionic surface sulfate groups from sulfuric acid hydrolysis and was in agreement with previous studies (Azzam, Heux, Putaux & Jean, 2010; Kargarzadeh, Ahmad,

Abdullah, Dufresne, Zainudin & Sheltami, 2012). In contrast, desulfated CNCs showed a positive ζ-potential of +24 mV under the same conditions, which was likely caused by an abundance of Na^+ cations at the slipping plane of the EDL that caused charge reversal of any trace amount of anionic sulfate groups. While ζ-potential experiments provided information about the nature of surface charges on unmodified and desulfated CNCs, DLS measurements were performed to determine their relative hydrodynamic diameter which could be correlated to their colloidal stability. As expected, unmodified CNCs displayed an equivalent spherical diameter of 141 nm, in accordance with previously reported values of cotton CNCs (Zoppe et al., 2014). Desulfated CNCs, on the other hand, were nearly impossible to obtain reproducible results, but in this case, was on the order of tens of microns. The value reported in Table 2 is not meant to be taken as absolute, but only to demonstrate the large difference in observable particle size after desulfation procedures. This effect is directly related to a large reduction in surface charge density after desulfation, and thus, their colloidal instability under these conditions. This evidence pointed to the fact that, although we observed a somewhat significant S 2p peak for desulfated CNCs in XPS (Figure 3), anionic surface charge from sulfate groups was significantly reduced by the desulfation procedures. It is noteworthy that under solvolytic desulfation with pyridinium salt in DMSO, no sulfur peak was observed by XPS (Jiang, Esker & Roman, 2010), but after seven repeated steps of acid-catalyzed desulfation, the surface charge density was decreased more than 5-fold, but sulfur was also still observed in XPS. Therefore, we could only speculate that the S 2p peak we observed was from sulfur of different chemical nature, and not derived from anionic sulfate groups. Gu et al. (Gu, Catchmark, Kaiser & Archibald, 2013) detected sulfur in cotton cellulose raw materials and their corresponding CNCs via combustion gas analysis. In both cases, this was unexpected, especially since CNCs were produced by hydrochloric acid hydrolysis. They proposed that trace amounts of sulfur remained in CNCs, which was derived from other plant tissues essential for plant biosynthesis. Therefore, we also speculated that the discrepencies we observed between XPS, conductometric titrations (Zoppe et al.,

2014) and ζ-potential were a result of sulfur in a different chemical state than that of anionic surface sulfate groups.

Table 2. ζ-potential and Z-average diameters of unmodified CNCs and desulfated CNCs. Values are expressed as an average of three measurements. Z-average diameters are considered as hydrodynamic diameters of equivalent spheres. (*Note: Z-average size of desulfated CNCs is only to demonstrate their colloidal instability)

Sample	ζ-potential (mV)	Z-average diameter (nm)
unmodified CNCs (sulfated)	-36.3 ± 1.5	141 ± 2
desulfated CNCs	+24.2 ± 1.7	14700 ± 5100*

A complementary tool to address the effectiveness of hydrolytic desulfation is by investigating the thermal stability of CNCs before and after treatments (Lin & Dufresne, 2014). Accordingly, TGA experiments were carried out to determing their degradation behavior. Shown in Figure 4 are % weight loss curves of unmodified CNCs and desulfated CNCs. Unmodified CNCs containing surface sulfate groups showed an onset of thermal degradation at *ca*. 220 °C within the range of ~150-350 °C, in agreement with previous reports (Lin & Dufresne, 2014; Zoppe et al., 2010). Contrarily, desulfated CNCs exhibited an onset of thermal degradation at *ca*. 285 °C and a more drastic negative slope in the range of 250-325 °C. This approximately 65 °C increase in onset temperature for desulfated CNCs clearly indicated there increased thermal stability upon removal of acidic sulfate groups. In the previous case of unmodified CNCs, the presence of acidic sulfate groups induced an autocatalytic degradation, which in turn, decreased their overall thermal stability. Overall, although XPS analysis of the S 2p signal of desulfated CNCs suggested inefficient base-catalyzed desulfation reactions, the evidence from conductometric titrations (Zoppe et al., 2014), TGA, DLS and ζ-potential strongly suggested that anionic surface sulfate groups were effectively

removed from CNCs. Nonetheless, the chemical state of sulfur in desulfated CNCs remains unclear, but is likely derived from other plant tissues essential for plant biosynthesis (Gu, Catchmark, Kaiser & Archibald, 2013).

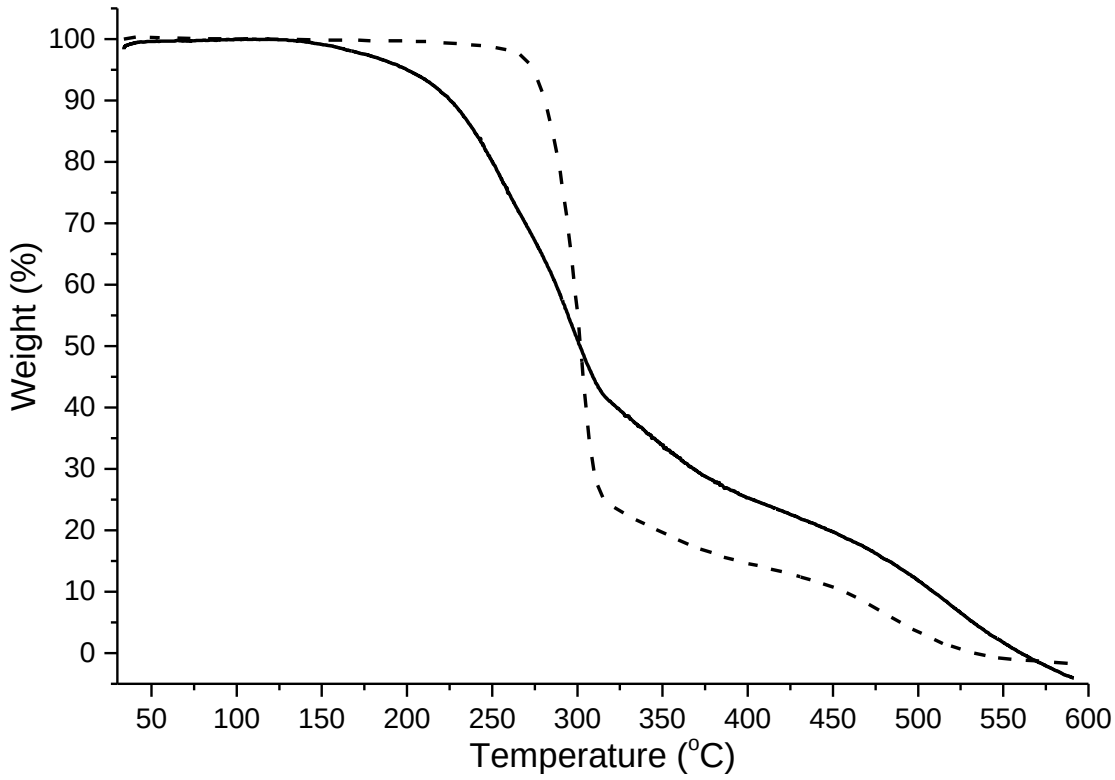

Figure 4. TGA curves of unmodified CNCs (solid line) and desulfated CNCs (dashed line).

3.5. XPS characterization of N 1s. Shown in Figure 5 are the N 1s regions of wide scan XPS spectra of CNCs before and after modifications. Desulfated CNCs displayed a trace amount of nitrogen, most likely from the adsorption of foreign contaminants during sample preparation. An increase in nitrogen peak intensity was observed for compound **3**, which was attributed to the secondary amine groups. In Table 1, it was also noted that the % N/O ratio increased from 0.23 to 0.71, as mentioned above. In the case of compound **4**, a slight shift to lower binding energy was observed, likely caused by secondary amine groups of the thiourea bonds, which were twice as abundant as the secondary amine groups closer to the CNC surface. The % N/O ratio showed a

393 marked increase to 1.2, that also supported the presence of additional nitrogen after reaction with 4-
394 SPITC. Carbon and oxygen high-resolution spectra of CNC samples were also recorded (shown in
395 Figure S2, S3, and Table S1). Compared to desulfated CNCs, compound **3** gave an increase in C1
396 peaks and C2/C3 ratio, attributed to C-C bonds of EBEA and CPSA. On the other hand, carbon
397 high-resolution spectra of compound **4** were unremarkable and mostly inconclusive, as the results
398 were similar to that of desulfated CNCs (see Figure S2 and Table S1). This was probably caused to
399 some degree by contamination of the C 1s signal, which is frequently encountered. Accordingly,
400 UV-Vis spectroscopy was later performed to further confirm the proposed structure of compound **4**.
401 It should be noted that quantifying small molecules on CNC surfaces has been historically
402 problematic, as in the case of ATRP initiators (Morandi & Thielemans, 2012; Zoppe et al., 2010),
403 since the number of surface cellulose chains is limited compared to the interior of crystallites. We
404 hope to address this issue in the future by further optimizing reactant stoichiometry and performing
405 elemental analysis in support of XPS measurements (Lin & Dufresne, 2014).
406

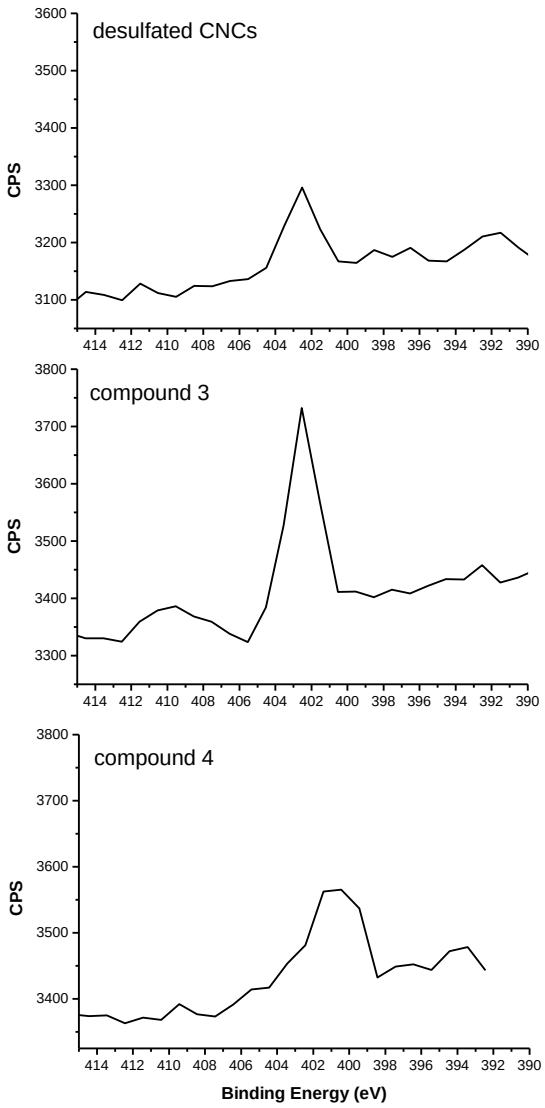

Figure 5. N 1s region of wide scan XPS spectra of desulfated CNCs (top), compound 3 (middle) and compound 4 (bottom).

3.6. UV-Vis spectroscopy of compound 4. UV-Vis spectroscopy was utilized to confirm FTIR observations of CNCs conjugated with phenyl sulfonate groups (compound **4**). Before analysis, compound **4** was exhaustively dialyzed against distilled water (7 days) to ensure removal of any unreacted 4-SPITC. Shown in Figure 6 is the relevant range of 200-375 nm of the UV-Vis spectra of unmodified CNCs, compound **4**, and 4-SPITC. A peak in UV absorbance was identified for 4-SPITC at 277 nm, which was also observed for compound **4** although at an expected lower

418 intensity. Dong *et al*. reported similar observations upon conjugation of CNCs with fluorescein-5'-
419 isothiocyanate (FITC) (Dong & Roman, 2007), although in our case no absorbance was observed at
420 higher wavelengths since 4-SPITC is not a fluorophore. UV-Vis spectroscopy provided a rapid and
421 facile method to detect conjugation of phenyl sulfonate ligands attached to CNC surfaces and one
422 could potentially develop standard calibration curves to quantify their surface coverage (Dong &
423 Roman, 2007; Nielsen, Eyley, Thielemans & Aylott, 2010). Here our objective was the proof of
424 concept that CNCs could be conjugated with antiviral ligands in aqueous media, therefore UV
425 calibration curves will be addressed in the future. Overall, the results of UV-Vis spectroscopy, XPS
426 and FTIR qualitatively confirmed the presence of phenyl sulfonate ligands and we propose that
427 these aqueous reaction pathways open new possibilities for conjugating CNCs with a diverse library
428 of target-specific functionalities.

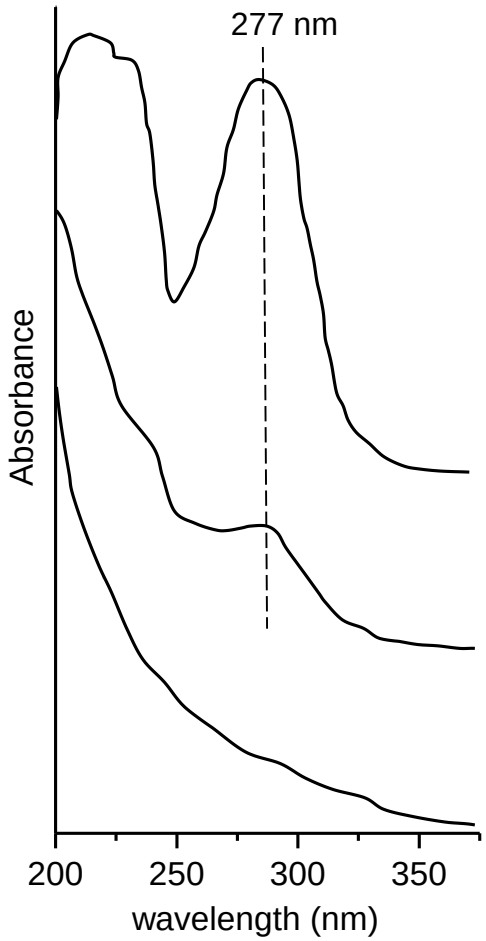

Figure 6. UV-Vis spectra (relevant range: 200-375 nm) of unmodified CNCs (bottom), compound **4** (middle) and 4-sulfophenyl isothiocyanate (4-SPITC) (top).

4. Conclusion

Due to the critical role of anionic sulfate groups in various biological processes, such as viral membrane fusion, cell signaling and adhesion, we have developed a simple aqueous-based procedure to create multivalent displays of "sulfate-mimicking" sulfonate groups on the surface of biocompatible CNCs. To this end, CNCs were decorated with model compounds containing sulfonate groups by taking advantage of epoxide and isothiocyanate chemistry, which were carried out in aqueous media under alkaline conditions. This approach may also find potential applications in facilitating surface-initiated ATRP when incorporated with desired initiators on surfaces presenting amine or hydroxyl groups (Zou, Kizhakkedathu & Brooks, 2009). Although

quantification of small molecules on the surface of CNCs was unsuccessful, the chemical reaction steps were followed by ATR-FTIR and UV-Vis spectroscopy. Additionally, XPS of N 1s and S 2p determined different binding energies which indicated different chemical environments that were used to confirm the proposed surface chemical structures. The base-catalyzed desulfation of CNCs was confirmed via dynamic light scattering (DLS), zeta potential measurements and thermogravimetric analysis (TGA). Based on this evidence, we concluded that the desulfation procedures significantly reduce the anionic charge of CNC surfaces, however the precise chemical nature of sulfur that was detected by XPS remains to be explored. Future studies should be directed at quantification of sulfonate ligands on CNCs surfaces by solid-state ^{13}C CP/MAS NMR and elemental analysis. We anticipate that with these facile aqueous procedures as the proof of concept, a diverse library of target-specific functionalities can be conjugated to CNCs for applications in nanomedicine, especially related to viral inhibition (Zoppe et al., 2014).

Acknowledgments

The authors would like to express their gratitude to Dr. Joseph Campbell for conducting XPS measurements and Cindy Känel for sample preparation and performing TGA analysis. The authors would also like to thank Prof. Harm-Anton Klok for use of the Molecular and Hybrid Materials Characterization Center (MHMC) at École Polytechnique Fédérale de Lausanne (EPFL). Funding support from Aalto University and EPFL, the Foundation for Finnish Inventions (Keksintösäätiö) and the Academy of Finland (Dec. No. 137759) are greatly appreciated.

References

Acharya, P., Dogo-Isonagie, C., LaLonde, J. M., Lam, S.-N., Leslie, G. J., Louder, M. K., Frye, L. L., Debnath, A. K., Greenwood, J. R., Luongo, T. S., Martin, L., Watts, K. S., Hoxie, J. A., Mascola, J. R., Bewley, C. A., & Kwong, P. D. (2011). Structure-Based Identification and Neutralization Mechanism of Tyrosine Sulfate Mimetics That Inhibit HIV-1 Entry. *ACS Chem. Biol.*, *6*(10), 1069-1077.

Azzam, F., Heux, L., Putaux, J. L., & Jean, B. (2010). Preparation By Grafting Onto, Characterization, and Properties of Thermally Responsive Polymer-Decorated Cellulose Nanocrystals. *Biomacromolecules, 11*(12), 3652-3659.

Baram-Pinto, D., Shukla, S., Gedanken, A., & Sarid, R. (2010). Inhibition of HSV-1 Attachment, Entry, and Cell-to-Cell Spread by Functionalized Multivalent Gold Nanoparticles. *Small, 6*(9), 1044-1050.

Baram-Pinto, D., Shukla, S., Perkas, N., Gedanken, A., & Sarid, R. (2009). Inhibition of Herpes Simplex Virus Type 1 Infection by Silver Nanoparticles Capped with Mercaptoethane Sulfonate. *Bioconjugate Chem., 20*(8), 1497-1502.

Beamson, G., & Briggs, D. (1992). *High Resolution XPS of Organic Polymers: The Scienta ESCA300 Database*. Chichester, England: Wiley & Sons.

Bernfield, M., Gotte, M., Park, P. W., Reizes, O., Fitzgerald, M. L., Lincecum, J., & Zako, M. (1999). Functions of cell surface heparan sulfate proteoglycans. *Annual Review of Biochemistry, 68*, 729-777.

Di Gianvincenzo, P., Marradi, M., Martinez-Avila, O. M., Bedoya, L. M., Alcami, J., & Penades, S. (2010). Gold nanoparticles capped with sulfate-ended ligands as anti-HIV agents. *Bioorg. Med. Chem. Lett., 20*(9), 2718-2721.

Dong, S., Hirani, A. A., Colacino, K. R., Lee, Y. W., & Roman, M. (2012). Cytotoxicity and Cellular Uptake of Cellulose Nanocrystals. *Nano LIFE, 2*(3), 1241006.

Dong, S., & Roman, M. (2007). Fluorescently Labeled Cellulose Nanocrystals for Bioimaging Applications. *J. Am. Chem. Soc., 129*(45), 13810-13811.

Farzan, M., Mirzabekov, T., Kolchinsky, P., Wyatt, R., Cayabyab, M., Gerard, N. P., Gerard, C., Sodroski, J., & Choe, H. (1999). Tyrosine sulfation of the amino terminus of CCR5 facilitates HIV-1 entry. *Cell (Cambridge, Mass.), 96*(5), 667-676.

Gericke, M., Liebert, T., & Heinze, T. (2009). Interaction of Ionic Liquids with Polysaccharides, 8-Synthesis of Cellulose Sulfates Suitable for Polyelectrolyte Complex Formation. *Macromolecular Bioscience, 9*(4), 343-353.

Grunwell, J. R., & Bertozzi, C. R. (2002). Carbohydrate Sulfotransferases of the GalNAc/Gal/GlcNAc6ST Family. *Biochemistry, 41*(44), 13117-13126.

Gu, J., Catchmark, J. M., Kaiser, E. Q., & Archibald, D. D. (2013). Quantification of cellulose nanowhiskers sulfate esterification levels. *Carbohydrate Polymers, 92*(2), 1809-1816.

Habibi, Y., Lucia, L. A., & Rojas, O. J. (2010). Cellulose Nanocrystals: Chemistry, Self-Assembly, and Applications. *Chem. Rev., 110*(6), 3479-3500.

Haensch, C., Hoeppener, S., & Schubert, U. S. (2010). Chemical modification of self-assembled silane based monolayers by surface reactions. *Chemical Society Reviews, 39*(6), 2323-2334.

Hermanson, G. T. (2008). *Bioconjugate Techniques*. London: Academic Press.

Hunter, R. J. (1981). *Zeta potential in colloids science*. New York: Academic Press.

Jackson, J. K., Letchford, K., Wasserman, B. Z., Ye, L., Hamad, W. Y., & Burt, H. M. (2011). The use of nanocrystalline cellulose for the binding and controlled release of drugs. *Int. J. Nanomed., 6*, 321-330.

Jiang, F., Esker, A. R., & Roman, M. (2010). Acid-Catalyzed and Solvolytic Desulfation of H2SO4-Hydrolyzed Cellulose Nanocrystals. *Langmuir, 26*(23), 17919-17925.

Johansson, L.-S., & Campbell, J. M. (2004). Reproducible XPS on biopolymers: Cellulose studies. *Surf. Interface Anal., 36*(8), 1018-1022.

Johansson, L.-S., Campbell, J. M., Koljonen, K., & Stenius, P. (1999). Evaluation of surface lignin on cellulose fibers with XPS. *Appl. Surf. Sci., 144-145*, 92-95.

Kargarzadeh, H., Ahmad, I., Abdullah, I., Dufresne, A., Zainudin, S. Y., & Sheltami, R. M. (2012). Effects of hydrolysis conditions on the morphology, crystallinity, and thermal stability of cellulose nanocrystals extracted from kenaf bast fibers. *Cellulose, 19*(3), 855-866.

Kloser, E., & Gray, D. G. (2010). Surface Grafting of Cellulose Nanocrystals with Poly(ethylene oxide) in Aqueous Media. *Langmuir, 26*(16), 13450-13456.

Lam, E., Male, K. B., Chong, J. H., Leung, A. C. W., & Luong, J. H. T. (2012). Applications of functionalized and nanoparticle-modified nanocrystalline cellulose. *Trends Biotechnol., 30*(5), 283-290.

Lin, N., & Dufresne, A. (2014). Surface chemistry, morphological analysis and properties of cellulose nanocrystals with gradiented sulfation degrees. *Nanoscale, 6*(10), 5384-5393.

Male, K., Leung, A., Montes, J., Kamen, A., & Luong, J. (2012). Probing inhibitory effects of nanocrystalline cellulose: inhibition versus surface charge. *Nanoscale, 4*(4), 1373-1379.

Moon, R. J., Martini, A., Nairn, J., Simonsen, J., & Youngblood, J. (2011). Cellulose nanomaterials review: structure, properties and nanocomposites. *Chem. Soc. Rev., 40*(7), 3941-3994.

Morandi, G., & Thielemans, W. (2012). Synthesis of cellulose nanocrystals bearing photocleavable grafts by ATRP. *Polymer Chemistry, 3*(6), 1402-1407.

Mueller, T. K. H., Cao, P., Ewert, S., Wohlgemuth, J., Liu, H., Willett, T. C., Theodosiou, E., Thomas, O. R. T., & Franzreb, M. (2013). Integrated system for temperature-controlled fast protein liquid chromatography comprising improved copolymer modified beaded agarose adsorbents and a travelling cooling zone reactor arrangement. *Journal of Chromatography A, 1285*, 97-109.

Ni, H., Zeng, S., Wu, J., Cheng, X., Luo, T., Wang, W., Zeng, W., & Chen, Y. (2012). Cellulose nanowhiskers: Preparation, characterization and cytotoxicity evaluation. *Bio-Med. Mater. Eng., 22*(1-3), 121-127.

Nielsen, L. J., Eyley, S., Thielemans, W., & Aylott, J. W. (2010). Dual fluorescent labelling of cellulose nanocrystals for pH sensing. *Chem. Commun. (Cambridge, U. K.), 46*(47), 8929-8931.

Pirrone, V., Wigdahl, B., & Krebs, F. C. (2011). The rise and fall of polyanionic inhibitors of the human immunodeficiency virus type 1. *Antiviral Res., 90*(3), 168-182.

Stone, M. J., Chuang, S., Hou, X., Shoham, M., & Zhu, J. Z. (2009). Tyrosine sulfation: an increasingly recognized post-translational modification of secreted proteins. *New Biotechnol., 25*(5), 299-317.

Wang, X., Ramstrom, O., & Yan, M. D. (2010). Quantitative Analysis of Multivalent Ligand Presentation on Gold Glyconanoparticles and the Impact on Lectin Binding. *Analytical Chemistry, 82*(21), 9082-9089.

Yamamoto, I., Takayama, K., Honma, K., Gonda, T., Matsuzaki, K., Hatanaka, K., Uryu, T., Yoshida, O., Nakashima, H., Yamamoto, N., Kaneko, Y., & Mimura, T. (1991). Synthesis, structure, and antiviral activity of sulfates of cellulose and its branched derivatives. *Carbohydr. Polym., 14*(1), 53-63.

Zoppe, J. O., Grosset, L., & Seppälä, J. (2013). Liquid crystalline thermosets based on anisotropic phases of cellulose nanocrystals. *Cellulose (Dordrecht, Neth.), 20*(5), 2569-2582.

Zoppe, J. O., Habibi, Y., Rojas, O. J., Venditti, R. A., Johansson, L.-S., Efimenko, K., Osterberg, M., & Laine, J. (2010). Poly(N-isopropylacrylamide) Brushes Grafted from Cellulose Nanocrystals via Surface-Initiated Single-Electron Transfer Living Radical Polymerization. *Biomacromolecules, 11*(10), 2683-2691.

Zoppe, J. O., Ruottinen, V., Ruotsalainen, J., Ronkko, S., Johansson, L. S., Hinkkanen, A., Jarvinen, K., & Seppala, J. (2014). Synthesis of Cellulose Nanocrystals Carrying Tyrosine Sulfate Mimetic Ligands and Inhibition of Alphavirus Infection. *Biomacromolecules, 15*(4), 1534-1542.

Zou, Y. Q., Kizhakkedathu, J. N., & Brooks, D. E. (2009). Surface Modification of Polyvinyl Chloride Sheets via Growth of Hydrophilic Polymer Brushes. *Macromolecules, 42*(9), 3258-3268.

567